Journal of Engineering, Project, and Production Management
2026, 16(5), 2025-292

Improved Multi-Scale CNN with Adaptive Weight Normalization for Closed-Loop Fault Diagnosis and Intelligent Recovery in Centralized Control Systems

Yi Xia[1], Yao Xu[2], Longgang Guo[3], Cheng Xie[4], Huan Ma[5], and Ling Weng[6]
[1] Senior engineer, State Grid Anhui Ultra High Voltage Company, Hefei, 231131, China, E-mail: xiayilol@163.com (corresponding author).
[2] Senior engineer, State Grid Anhui Ultra High Voltage Company, Hefei, 231131, China, E-mail: xuy221x@ah.sgcc.com.cn
[3] Senior engineer, State Grid Anhui Ultra High Voltage Company, Hefei, 231131, China, E-mail: guolongg0317@ah.sgcc.com.cn
[4] State Grid Anhui Electric Power Co., Ltd., Hefei 230022, China, E-mail: xiec0222@ah.sgcc.com.cn
[5] Engineer, State Grid Anhui Ultra High Voltage Company, Hefei, 231131, China, E-mail: ahdlmahuan@163.com.cn
[6] Senior engineer, State Grid Anhui Ultra High Voltage Company, Hefei, 231131, China, E-mail: wengl0611@ah.sgcc.com.cn

Project Management
Received November 27, 2025; revised January 6, 2026; accepted January 14, 2026
Available online June 17, 2026

Abstract: Traditional centralized control systems often struggle to extract discriminative features from complex multi-source signals, leading to delays in fault diagnosis and suboptimal recovery performance. To address this, we propose an improved Convolutional Neural Network (CNN) architecture that integrates multi-scale convolutional kernels to capture heterogeneous spatiotemporal patterns. An adaptive weight normalization mechanism recalibrates feature channel responses, enhancing the detection of subtle anomalies. Extracted features are aggregated via global average pooling and classified by a softmax layer to identify fault types. The diagnosis results are then forwarded to an intelligent control module, where a parameter reconfiguration algorithm adjusts control strategies and regenerates execution commands, thereby establishing a closed-loop, self-adaptive recovery framework. Unlike existing studies that focus solely on either fault diagnosis or fault-tolerant control, this work explicitly integrates multi-scale feature learning and adaptive parameter reconfiguration within a unified closed-loop architecture, forming a system-level coupling between perception and recovery rather than introducing an isolated algorithmic improvement. Experiments on a centralized control simulation platform show that the proposed method achieves a fault classification accuracy of 95.2%, with an average diagnostic response time of 0.42s. Under extreme anomaly conditions, the system maintains a recovery stability index of 0.89. This study shifts centralized control from passive monitoring to proactive intelligent perception and self-healing control, offering a viable technical pathway for high-reliability industrial operation.

Keywords: Convolutional neural network, centralized control system, fault diagnosis, adaptive weight normalization, intelligent recovery.

DOI 10.32738/JEPPM-2025-292

1. Introduction

A centralized control system collects, monitors, and dispatches information from distributed equipment through a central control center, thereby enabling centralized control of the process (Arabpour and Hojabri, 2023; Dantzer and Kerkez, 2025; Meng et al., 2024). The core issue is to effectively extract features from complex multi-source signals to achieve accurate diagnosis and rapid recovery. With the increase in system scale and complexity, the coupling relationships and signal interactions between devices are becoming increasingly dense, and higher requirements for system operation stability and safety(Almihat and Kahn, 2023; Liu, 2023; Wang, 2021). Research on intelligent fault diagnosis and recovery mechanisms for centralized control systems is of great significance for improving industrial production continuity, reducing equipment loss, and reducing operation and maintenance costs (Li, 2022; Liu, 2022; Yan et al., 2023). The application of deep learning provides a new technical solution for realizing system-level self-perception and self-healing control.

The current centralized control system's fault diagnosis and recovery face many technical problems. The nonlinear characteristics of multi-source heterogeneous signals make it difficult for traditional feature extraction methods to achieve stable modeling (Chen, 2024; Jin, 2022). Current centralized control system fault diagnosis and recovery faces two technical problems: first, the feature extraction method is not very sensitive to complex signals. Second, the diagnosis and recovery process lacks an information closure loop. The two problems directly limit the system's development of intelligence. Sensor data is cross-interfered in both temporal and spatial dimensions, leading to high-dimensional sparsity in fault signatures (Wan, 2023; Zhao et al., 2024). Some studies have shown that fault signals under complex operating conditions can be buried in the noise superposition and lead to misidentification (Lee, 2024; Wang and Cao, 2023). Data imbalance also prevents models from adequately learning minority faults during training (Jalayer, 2022; Kafunah and Breslin, 2021). The recovery process of centralized control systems requires extremely high real-time performance and stability, and traditional control strategies are prone to decision conflicts or recovery lags when multiple failures occur (Ahmadi, 2022; Han, 2023). Such methods have limited accuracy in extracting abnormal patterns at the feature level and lack effective transfer of diagnostic results to recovery strategies at the system level, making it difficult to form a stable fault diagnosis-control-recovery closed loop. These issues collectively limit the effective construction of intelligent diagnostic systems and the system's rapid self-healing capabilities.

Existing research has explored improving fault diagnosis and recovery methods. Pattern recognition methods based on Support Vector Machines (SVMs) rely on manual feature extraction, are sensitive to noise, and have limited generalization capabilities (Lei, 2025; Zhang et al., 2024). Hierarchical learning methods based on deep belief networks take a long time to train for high-dimensional feature recognition and are prone to falling into local optima. Long Short-Term Memory (LSTM) networks perform well in time series signal analysis but are limited in capturing spatial features (Yu et al., 2024; Zhang et al., 2025). Although autoencoder structures can learn unsupervised features, the reconstruction error is unstable for complex signals. These methods improve the accuracy of single-fault type recognition. However, it remains challenging to achieve high-precision diagnosis and rapid recovery under multi-source data conditions, and a real-time, intelligent self-healing mechanism for centralized control systems has not yet been established (Du et al., 2023; Zhang, 2023).

To address the problems of insufficient feature extraction and delayed recovery response in traditional methods, this paper proposes an improved CNN method that extracts spatiotemporal features of multi-source signals via a multi-scale convolutional kernel structure and applies an adaptive weight normalization mechanism in the convolutional layer to dynamically adjust feature channel weights. The model takes the raw operating signal as input, extracts features using a multi-scale convolutional unit, and then passes them to the feature fusion layer for unified representation. Global average pooling and a softmax classifier are then used to determine the fault type. The diagnostic results are fed into the intelligent control module, which uses a parameter reconfiguration algorithm to adjust the control path and execute instructions to restore the system. The diagnostic and recovery architecture constructed in this paper achieves closed-loop control from fault identification to strategic recovery. This study is guided by three research questions: whether multi-scale convolution can maintain discriminative fault features under multi-source signal coupling, whether adaptive normalization stabilizes feature distributions across heterogeneous sensors, and whether embedding diagnostic results into parameter reconfiguration logic improves recovery timeliness and system-level control stability. The originality of this research lies not in proposing new convolution operators or control laws, but in constructing a tightly coupled diagnostic-control framework. Within this framework, fault classification outputs are structurally embedded into adaptive recovery logic, thereby achieving system-level cooperative behavior lacking in existing modular methods. This architecture implements fault diagnosis and recovery control as two functionally separated layers: the diagnostic layer is responsible for state identification and fault labeling based on signal characteristics. In contrast, the control layer specifically utilizes the diagnostic output as decision input to achieve parameter reconstruction, rather than sharing the original signal representation.

2. Fault Diagnosis and Intelligent Recovery Model based on Improved CNN

2.1. Improved Convolutional Neural Network Structure Design

The multi-source signals of the centralized control system fluctuate frequently in time and are spatially coupled across devices. Temperature, current, and pressure signals exhibit nonlinear dependencies, and local disturbances are transmitted via time lags (Qin et al., 2023; Wenyun et al., 2022; Yongqiang et al., 2023). To characterize this cross-scale propagation feature, this paper designs a multi-scale convolution kernel fusion structure to enable the network to analyze local anomalies and system trends at the same layer (Gao et al., 2022; Yang et al., 2022; Zou et al., 2025). Small-scale convolution kernels extract high-frequency disturbances of current and vibration, while large-scale convolution kernels capture low-frequency changes across work sections. The fusion stage achieves a dynamic balance of multi-dimensional information through a weighted combination. The process is expressed as:

$$F_t = \sum_{i=1}^{N} \lambda_i \cdot (S_t * K_i) \tag{1}$$

In Eq. (1), St represents the multi-source signal matrix collected at time t, which includes operating parameters such as temperature, current, pressure, and vibration; Ki is the convolution kernel of the i-th scale, $*$ represents the convolution operation; λ i is the fusion weight, which controls the contribution ratio of each scale feature to the output. Ft represents the multi-scale feature map after fusion. This formula reflects the network's weighted responses to different dynamic modes in the multi-source signal, thereby retaining the weak disturbance during the fault-induction stage in the multi-scale domain.

Multi-source signals have dimensional differences and random noise interference at the sensor end. If they are directly superimposed, the distribution of feature channel responses is unbalanced, thereby affecting the directional stability of the

convolution kernel weight update (Deng et al., 2023; Jin et al., 2021). To maintain a balanced distribution of feature space during training, the network uses an adaptive weight normalization mechanism across convolutional layers. This mechanism statistically normalizes each channel's output and combines learnable parameters to recalibrate the amplitude, ensuring the feature channel maintains a dynamic balance of signal energy. The normalization process is defined as:

$$\widehat{X}_{c,t}=\frac{X_{c,t}-\mu_c}{\sqrt{\sigma_c^2+\epsilon}}\cdot\alpha_c+\beta_c \tag{2}$$

In Eq. (2), Xc,t represents the convolution output of the c-th feature channel at time t, μc and σc2 are the mean and variance of the channel, ϵ is a stability constant to prevent zero division errors, αc and βc are trainable parameters for adaptive scaling and offset correction, and Xc,t represents the normalized feature. This process ensures the comparability of different sensor signals in the numerical domain, enabling the network to maintain consistent feature responses despite amplitude drift or noise.

After the convolution and normalization, networks must compress high-dimensional spatiotemporal features into a stable state vector for the fault classifier to determine the device's operating status (Guo et al., 2023; Han et al., 2023). The global average pooling layer here serves as a system-level feature aggregator. It converts the complex signal flow into a statistical representation of the control state by averaging feature responses across time and space. This process is expressed as:

$$g_c=\frac{1}{T\times M}\sum_{t=1}^{T}\sum_{m=1}^{M}\widehat{X}_{c,t,m} \tag{3}$$

In Eq. (3), T is the length of the time series, M is the number of sensor space dimensions, Xc,t,m represents the characteristic response of the c-th channel at time t and spatial dimension m, and gc is the global average pooling output, which reflects the steady-state characteristics of the control system within a certain time window and serves as the input vector for subsequent fault classification. Through this process, the system's abnormal patterns are mapped to a set of measurable operational characteristics, providing an interpretable basis for decision-making for the intelligent recovery module.

In centralized control scenarios, the improved CNN performs a three-stage process: multi-scale signal fusion, adaptive feature correction, and spatiotemporal aggregation. The multi-scale convolutional layer simultaneously identifies local disturbances and system trends; the adaptive normalization mechanism maintains feature balance across different sensor sources; and the global pooling layer maps dynamic signals into stable state representations, forming a bridge between fault identification and control feedback. The overall network structure is shown in Fig. 1. The left side shows the multi-source signal input layer, the multi-scale convolution and adaptive normalization structure, the fault classification module, and the intelligent recovery module. Signals flowing through each module form a closed loop of diagnosis and control, enabling embedded collaboration of the system's self-healing logic.

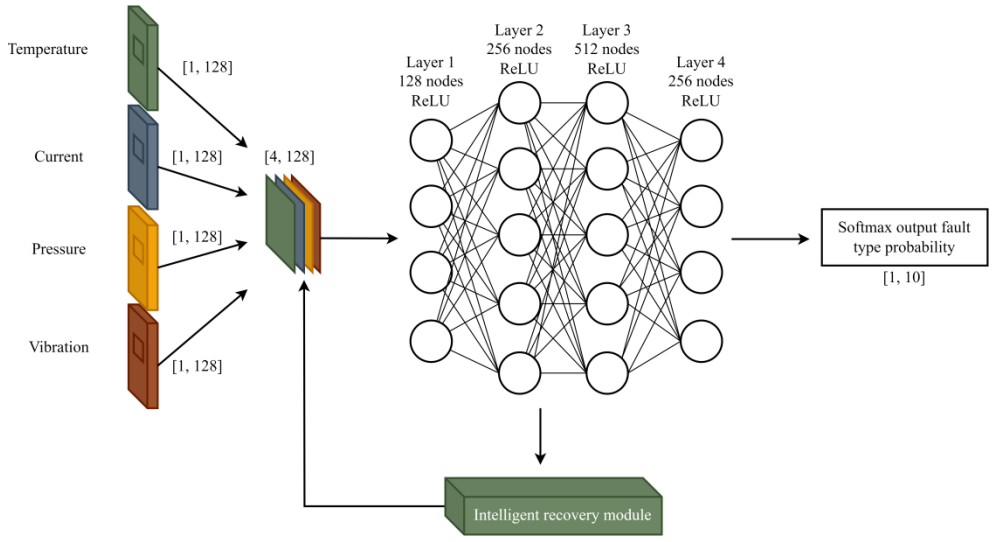

Fig. 1. Improved CNN overall structure framework

2.2. Implementation of Fault Diagnosis and Classification Module

The fault diagnosis and classification module receives the fused multi-scale feature map and uses a multi-layer Softmax discriminant network to classify faults. This module uses the steady-state feature vector of the power grid centralized control

signal as input and establishes the classification decision boundary through linear mapping and a normalized exponential function to distinguish different equipment states. The output of the Softmax classifier is calculated as follows:

$$P(y_j|F_t)=\frac{\exp(W_jF_t+b_j)}{\sum_{k=1}^{C}\exp(W_kF_t+b_k)} \tag{4}$$

In Eq. (4), W_j and b_j are the weight matrix and bias term corresponding to the j-th class, respectively. C is the total number of fault types. $P(y_j|F_t)$ represents the probability that the input feature belongs to the j-th class fault.

The classification layer uses cross-entropy loss to approximate the true label distribution. Adam optimizer accelerates the convergence and improves the robustness to non-stationary signals. The early stopping mechanism prevents overfitting to the minority class. Outputting fault category and confidence level provides accurate status information to the intelligent recovery module, enabling fast diagnosis and location. The diagnostic module outputs discrete fault category labels and corresponding confidence scores as high-level state descriptors, serving as the sole interface variables passed to the intelligent recovery layer, thereby isolating feature extraction from control execution.

2.3. Intelligent Recovery and Parameter Reconfiguration Mechanism

After receiving fault category labels and confidence scores from the diagnostic layer, the intelligent recovery module performs parameter reconfiguration without direct access to raw sensor signals or intermediate feature maps, ensuring functional separation between perception and control. This mechanism adjusts the weight matrix for key control variables in an online manner. The affected nodes can recover and still guarantee global stability when only a small portion of them operate under reconfigured parameters. The parameter reconfiguration can be written as:

$$\Theta_{t+1}=\Theta_t-\eta\cdot R(y_j)\cdot\nabla_{\Theta_t}L(F_t,y_j) \tag{5}$$

In Eq. (5), Θ_t represents the system control parameter matrix at time t, η is the adaptive update step size, $L(F_t,y_j)$ is the loss function based on the classification result, reflecting the degree to which the current control state deviates from the normal operating condition, and $R(y_j)$ is the recovery response coefficient for fault type y_j, which is used to adjust the recovery speed and direction under different types of faults. The loss function is defined in the form of weighted square error:

$$L(F_t,y_j)=\sum_{i=1}^{n}\alpha_i\left[u_i(t)-u_i^*(t)\right]^2 \tag{6}$$

In Eq. (6), $u_i(t)$ represents the actual output of the i-th control variable at time t, $u_i^*(t)$ represents the expected steady-state value of the control variable under normal operating conditions, and α_i is the control variable weight coefficient, which is used to reflect the impact of different variables on system stability. The design of $R(y_j)$ is based on the statistical characteristics of the fault classification results and is defined as:

$$R(y_j)=\beta_j(1+\gamma_j\delta_j) \tag{7}$$

In Eq. (7), β_j represents the basic recovery weight for category j, δ_j is the normalized average loss for this type of fault during the training phase, and γ_j is the adjustment coefficient used to control the response sensitivity under different fault types. This design enables parameter reconfiguration with differentiated adjustment capabilities across different fault scenarios, ensuring that the recovery process completes local adjustments while maintaining global stability. The adaptive recovery process follows a monotonic error reduction principle, with the parameter update direction constrained by the deviation between the actual and expected steady-state outputs. Since the update magnitude is bounded by the recovery response coefficient and the adaptive step size, the closed-loop system converges to a bounded equilibrium region rather than diverging during repeated adjustments. This design ensures that recovery actions remain confined within a stable operating envelope during fault compensation. At the system level, this mapping establishes a one-directional decision flow from diagnosis to control within each recovery cycle, preventing feedback interference between learning-based perception and rule-constrained control actions.

3. Experiment and Result Analysis

3.1. Experimental Design and Data Description

Experiment on the centralized control system simulation platform. The centralized control system simulation platform includes a signal acquisition module, a data preprocessing module and a model training and inference module. This work aims to verify the accuracy of fault diagnosis and recovery control using an improved convolutional neural network on multi-source industrial signals. Experimental signals are collected in industrial process control. Data are collected from the sensor node's temperature, current, pressure, and vibration sensors. Each signal type is sampled in normal and various fault conditions. The sampling frequency is 1 kHz, and the data length per channel is 1024. After signal acquisition, normalization, and segmentation, the time-domain sliding window is used to generate the training sample set, and then input into the model. Signal normalization uses channel-wise statistical scaling to align each sensor stream to a zero-centered distribution with controlled variance, ensuring numerical consistency across heterogeneous signal sources before convolutional processing. The dataset contains 12000 samples, and 70% are used for the training set, 20% for the validation set, and 10% for the test set.

The experimental hardware environment is a GPU-accelerated Linux server. The graphics card is NVIDIA RTX 4090, the processor is Intel Xeon W-2295, and the memory is 128 GB. The software environment uses Python 3.10, TensorFlow 2.15 and CUDA 12.2. The initial training batch size is 32, and the maximum number of iterations is 200. To achieve stable convergence, a learning rate decay strategy is adopted. That is, if the accuracy over five consecutive runs on the validation set does not improve, the learning rate is automatically decayed. The cross-entropy function is adopted as the loss function, and Adam is adopted as the optimizer. The input signal passes through five convolutional layers with channel sizes progressively expanded according to the channel growth rate, where each layer applies parallel convolution kernels of sizes three by three, five by five, and seven by seven, followed by adaptive normalization and rectified linear activation. Finally, the output can pass through global average pooling and then be fed to the Softmax classifier for fault determination.

The initial values and adjustment ranges of the model parameters are gradually optimized during the training phase based on validation set performance. Table 1 lists the core hyperparameter configurations involved in network training, including the adjustment process from initialization to final value determination.

Table 1. Main parameter configuration of improved CNN model

Parameter Item	Initial Value	Adjustment Range	Final Value
Learning rate	1×10^{-3}	1×10^{-4}–1×10^{-3}	8×10^{-4}
Batch size	32	32–128	64
Convolution kernel size	[3×3, 5×5, 7×7]	Fixed	[3×3, 5×5, 7×7]
Number of convolutional layers	4	3–6	5
Channel growth rate	1.5	1.0–2.0	1.6
Normalization momentum coefficient	0.9	0.8–0.95	0.92
Dropout rate	0.3	0.1–0.5	0.25
Optimizer	Adam	Fixed	Adam
Activation function	ReLU	Fixed	ReLU
Maximum training epochs	200	100–300	180

3.2. Fault Identification Performance Analysis

The experimental part uses multi-source operating signals from the centralized control system as input and constructs an improved convolutional neural network to classify and identify typical faults. The fault types include five representative operating conditions: F1 is sensor drift, F2 is actuator failure, F3 is communication anomaly, F4 is energy overload, and F5 is control logic anomaly. Each category contains 100 samples. After training, the model's recognition performance was verified using a test set. A confusion matrix was constructed from the predicted outputs and the true labels. The recognition results are shown in Fig. 2.

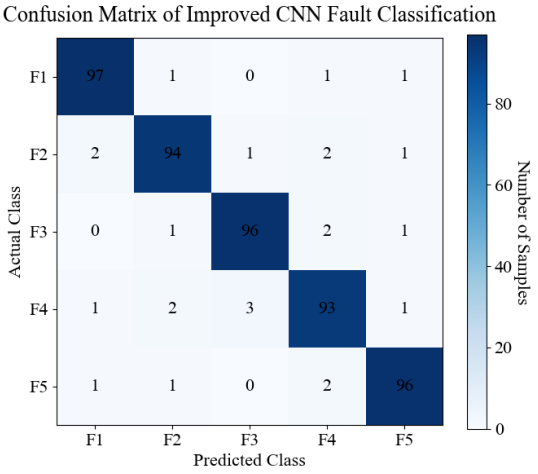

Fig. 2. Fault identification results

Fig. 2 shows that the F1 category achieved 97% accuracy, primarily because the low-frequency stability of the sensor drift signal makes it easy for the convolutional layer to extract this trend information. The F4 category achieved 93% accuracy, the lowest of all categories. This is because the energy overload fault signal is influenced by fluctuations in load and equipment operating conditions, and the high feature overlap across the local receptive fields of multi-scale convolution kernels leads to feature confusion. The stable accuracy of F2, F3, and F5 categories was 94%, 96%, and 96%, respectively. This indicates that the adaptive normalization mechanism can maintain the discriminability of feature distribution and

suppress the noise interference. The overall recognition accuracy was 95.2%, further demonstrating the improved diagnostic accuracy of the CNN under complex operating conditions.

3.3. Analysis of Diagnostic Response Efficiency

This paper designs and tests the response performance of five typical models under different signal dimensions. The comparison models include SVM, LSTM, traditional CNN, improved CNN (without a normalization mechanism), and improved CNN with an adaptive weight normalization. SVM, as a traditional shallow classification model, relies on manual feature extraction and suffers from high response delays in high-dimensional signals. The LSTM has the ability to model time series, but its large number of parameters limits its inference speed. Traditional CNNs can achieve good results in spatial feature extraction, but their performance is unstable under multi-source signal interference. CNN improves feature extraction efficiency by optimizing the convolution kernel structure. On this basis, the model with an adaptive weight normalization mechanism can dynamically adjust feature channels, thereby further reducing computational redundancy and improving timing response performance. The experiment measured the average diagnostic response time for each model and the trend in response time as the signal dimension expanded. The results are shown in Fig. 3.

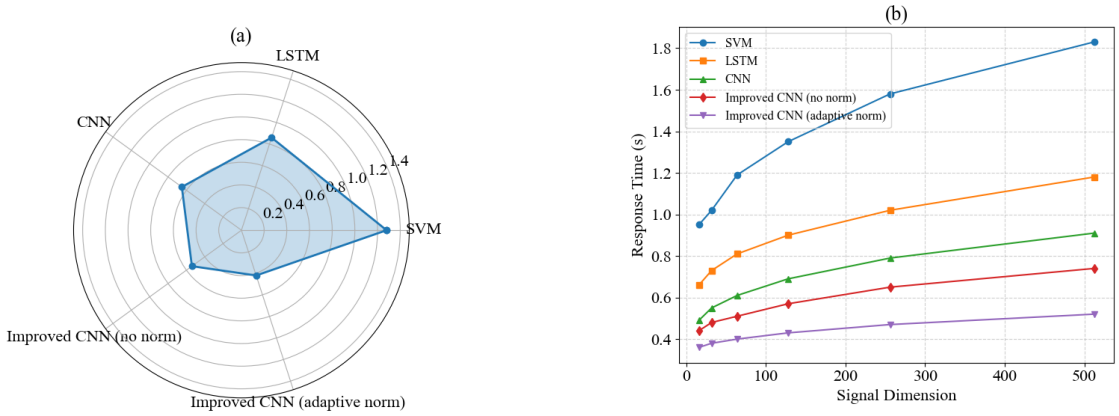

(a) Comparison of average diagnostic response time for different models

(b) Trends in diagnostic response time at different signal dimensions

Fig. 3. Analysis of diagnostic response efficiency of the improved CNN model

As shown in Fig. 3, the average response time for the SVM is 1.28 seconds, the LSTM is 0.86 seconds, the traditional CNN is 0.65 seconds, the improved CNN (without normalization) is 0.54 seconds, and the improved CNN with an adaptive normalization mechanism is only 0.42 seconds. This is due to differences in feature processing and parameter updating. Due to the lack of a parallel feature mapping structure, the SVM relies on global optimization, resulting in increased computational overhead when operating with multiple signal sources. During time series unrolling, the LSTM accumulates state dependencies, and the parameter update process has a long backpropagation path, resulting in relatively high response latency. Although the traditional CNN has a parallel convolutional structure, the fixed size of the convolutional kernel leads to redundant computation when extracting local anomalies from complex signals. The improved CNN alleviates the problem of duplicate local feature extraction by combining multi-scale convolutions and reducing latency in inter-layer data transmission. In addition, the adaptive normalization mechanism further adjusts the distribution of channel weights and uses effective features in forward propagation. With the increase in signal dimension from 16 to 512, the response time of each model increases. The SVM response time increases from 0.95 seconds to 1.83 seconds, and the improved CNN response time (including normalization) increases from 0.36 seconds to 0.52 seconds. This indicates that the parameter normalization mechanism reduces the computational amount caused by the redundancy of effective features in a high-dimensional signal. Overall, results show that network structure optimization and adaptive weight adjustment can reduce diagnostic response latency, enable the model to run stably in a real-time diagnostic application, and achieve high accuracy.

To isolate the contribution of each architectural component, an ablation experiment was conducted by selectively removing multi-scale convolution, adaptive normalization, and recovery control coupling while keeping other settings unchanged. The classification accuracy and response time were recorded for each configuration. The results are shown in Table 2.

3.4. Intelligent Recovery Performance Analysis

In the intelligent recovery performance verification experiment, the system has been dynamically recovered from a variety of typical fault scenarios, including sensor signal faults, execution unit jamming, communication link delays, control parameter drift, and power module failures. The experiment was carried out on the unified centralized control simulation platform. The fault injection intensity was divided into five levels. Level 1 is a slight disturbance, Level 2 is medium-low disturbance, Level 3 is medium anomaly, Level 4 is high intensity unstable, and Level 5 is extreme anomaly. This is to evaluate the response and stability performance of the intelligent recovery algorithm under different complexities. During the test, the recovery time and stability index after recovery were recorded. By comparing the response characteristics of the

traditional control strategy and the improved algorithm, a quantitative relationship for recovery performance was established. The experimental results are shown in Fig. 4.

Fig. 4 shows the results of the experiments. When sensor signal anomalies and communication link delays occur, the average recovery time of the traditional control strategy is 1.28s and 1.54s, respectively, while the average recovery time of the intelligent recovery algorithm is only 0.4s and 0.57s, respectively. The control path reconfiguration adaptively adjusts the execution unit. Therefore, it can reduce redundant instruction delay by adjusting execution unit parameters in real time. When the execution unit is stuck and a power module fails, the intelligent recovery algorithm can maintain average recovery times of 0.63s and 0.68s. It can maintain high computational parallelism and signal synchronization even under high computational load. When the fault is level 5, the stability index of the traditional strategy is 0.55. The stability index of the intelligent recovery algorithm is 0.89. The adaptive feature-weight mechanism suppresses the propagation error of a high-disturbance signal. It can suppress the propagation error of a high-disturbance signal and maintain the dynamic consistency of the control loop. Finally, an improved algorithm can maintain and achieve a highly reliable recovery speed and stability under multi-source signal interference and complex operating conditions.

3.5. Extended Experimental Validation of Robustness, Stability, and Scalability

The conclusions regarding robustness, long-term stability, and scalability require validation beyond single-fault and short-duration experiments. To address this, extended experiments are conducted under compound fault scenarios, prolonged continuous operation, and increasing system scale. Quantitative results are summarized in Tables 3 and 4 and analyzed to assess whether the proposed framework maintains bounded recovery behavior under more demanding conditions. Robustness under fault interaction is examined by injecting multiple fault types within the same control cycle. The recovery performance under compound fault conditions is summarized in Table 3, where both recovery time and post-recovery stability are reported for different fault combinations.

As shown in Table 3, recovery time increases gradually as fault coupling becomes more complex, while the stability index remains within a constrained range across all scenarios. Even in the triple fault case, the stability index does not collapse below the level observed in single-fault high-intensity experiments. This indicates that the adaptive recovery mechanism preserves bounded response characteristics under interacting disturbances, providing experimental support for the robustness-related conclusions.

To validate long-term stability and scalability, the centralized control system is continuously operated under periodic fault injection as the number of sensor nodes increases. The corresponding recovery performance over twelve hours of operation is reported in Table 4.

Table 2. Ablation study results of model components

Model configuration	Accuracy (%)	Response time (s)
Full proposed model	95.2	0.42
Without adaptive normalization	92.6	0.54
Without multi-scale convolution	91.8	0.58
Without recovery control coupling	93.1	0.47

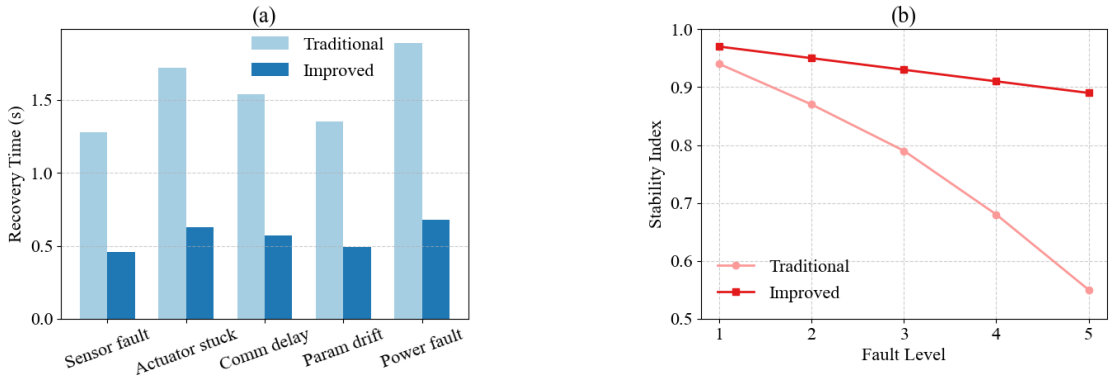

(a) Comparison of recovery time for different fault types

(b) Changes in system stability for different fault intensities

Fig. 4. Comparison of intelligent recovery performance

Table 3. Recovery performance under multi-fault coupling scenarios

Fault combination	Average recovery time (s)	Stability index
Sensor drift + communication delay	0.61	0.86
Actuator jamming + parameter drift	0.68	0.84
Energy overload + logic anomaly	0.72	0.82
Triple fault coupling	0.79	0.80

Table 4. Long-duration operation and scalability evaluation

Number of sensor nodes	Operation duration (h)	Average recovery time (s)	Stability index
64	12	0.45	0.90
128	12	0.47	0.89
256	12	0.50	0.88
512	12	0.54	0.87

As shown in Table 4, recovery time increases gradually as fault coupling becomes more complex, while the stability index remains within a constrained range across all scenarios. Even in the triple fault case, the stability index does not collapse below the level observed in single-fault high-intensity experiments. This indicates that the adaptive recovery mechanism preserves bounded response characteristics under interacting disturbances, providing experimental support for the robustness-related conclusions.

4. Discussion on Theoretical and Practical Implications

The experimental results demonstrate improvements in diagnostic efficiency and recovery performance. However, learning-based closed-loop control systems require explicit discussion of stability, convergence, and fault-tolerance properties. This section analyzes the theoretical implications of the proposed framework at the system level and discusses the practical consequences of diagnostic uncertainty within the closed control loop.

From a control perspective, the stability of the proposed framework is determined by the boundedness of the parameter reconfiguration process rather than the neural network's internal convergence. The adaptive update of control parameters is constrained by predefined step sizes and recovery coefficients, ensuring that each adjustment remains within an admissible operational region. As a result, repeated recovery actions do not lead to unbounded state divergence, and the closed-loop system converges to a stable operating neighborhood rather than a single equilibrium point. This design implies convergence in a practical sense, where control variables settle within tolerable deviation limits rather than asymptotically approaching an ideal state.

Fault-tolerance in the proposed framework is achieved through structural separation between diagnostic inference and control execution. The diagnostic module provides discrete fault labels and confidence scores, while the recovery module applies parameter reconfiguration under fixed safety constraints. This separation prevents classification uncertainty from directly amplifying control actions. Even under imperfect diagnostic outcomes, recovery adjustments are moderated by loss-based deviation measures, which restrict excessive parameter variation and preserve system-level robustness.

Misclassification within the diagnostic module may lead to suboptimal recovery paths. Although its impact on system stability is limited by the closed-loop design. When an incorrect fault category is selected, the recovery mechanism applies conservative parameter adjustments based on output deviation rather than on categorical identity alone. As a result, the system response manifests as delayed convergence rather than destabilization. Experimental observations in multi-fault and long-duration tests indicate that such misclassification does not trigger oscillatory control behavior or cumulative instability, but instead results in bounded transient performance degradation.

From a practical standpoint, these properties indicate that the proposed framework is suitable for deployment in centralized control environments where diagnostic uncertainty is unavoidable. The combination of bounded adaptive recovery, structural decoupling, and deviation-driven control logic ensures that performance degradation caused by learning errors remains manageable, supporting reliable operation under realistic industrial conditions.

5. Conclusion

The improved CNN in this paper performs deep feature extraction and dynamic balance correction of multi-source signals in a centralized control system via a multi-scale convolutional kernel structure and an adaptive weight normalization mechanism. The experimental results show that the model achieves an overall fault recognition accuracy of 95.2% and an average response time of 0.42s. In the intelligent recovery test, the system achieved average recovery times of only 0.57s and 0.63s under conditions of communication, link delay, and execution unit jamming, respectively. After recovery, the system stability index is above 0.89. Experimental results verified that the multi-scale convolutional structure can capture cross-device coupling features in multiple ways. The adaptive normalization mechanism can maintain feature distribution consistency and parameter update stability in the presence of signal interference. This method can suppress interference from multi-source signals and improve the reliability, timely recovery, and adaptability of the control path. It can maintain high recovery speed and stability under multi-source signal interference and complex operating conditions. It provides a feasible technical solution for achieving autonomous perception and intelligent recovery in industrial automation. This study has certain limitations. The experimental data come from a centralized control simulation platform, thus, signal quality and noise characteristics are constrained by predefined settings. While multi-source signals are considered, severe sensor degradation and extreme noise contamination are not fully explored. Moreover, the fault categories are constructed under controlled distributions, and the impact of strong class imbalance on diagnostic robustness needs further investigation. The proposed model is validated in a specific centralized control scenario; its generalization to other industrial systems with different architectures and operating conditions requires further examination.

Author Contributions

Yi Xia contributed to conceptualization, methodology, supervision, project administration, validation, manuscript editing, and overall coordination of the research. Yao Xu contributed to conceptualization, methodology, analysis, investigation, and manuscript editing. Longgang Guo contributed to methodology, software, validation, data curation, and draft preparation. Cheng Xie contributed to investigation, data collection, draft preparation, and visualization. Huan Ma contributed to data collection, software, visualization, and draft preparation. Ling Weng contributed to methodology, validation, analysis, and manuscript editing. All authors have read and agreed with the manuscript before its submission and publication.

Funding

This research received no specific financial support from any funding agency.

Institutional Review Board Statement

Not applicable.

Declaration of Artificial Intelligence (AI) Tools

The authors used AI tools solely for language editing and readability improvement. The authors reviewed and verified all content and take full responsibility for the accuracy and integrity of the manuscript.

References

Ahmadi, S. (2022). A Real-Time Fault-Tolerant Control Approach to Ensure the Resiliency of a Self-Healing Multilevel Converter. *Energies,* 15(13), 4721-4742.

Almihat, M., and Kahn, E. (2023). Centralized control system for islanded minigrid. *AIMS Energy*, 11(4), 663-682.

Arabpour, A., and Hojabri, H. (2023). An improved centralized/decentralized accurate reactive power sharing method in AC microgrids. *International Journal of Electrical Power & Energy Systems,* 148(1), 108908-108913.

Chen, D. (2024). A real-time fault diagnosis method for multi-source heterogeneous information fusion based on two-Level transfer learning. *Entropy*, 26(12), 1007-1028.

Dantzer, A., and Kerkez, B. (2025). Teamwork without talking: distributed system estimates maintain approximately centralized control of smart urban drainage systems during communications outages. *Water Research X*, 26(1), 100287-100291.

Deng, C., Deng, Z., Lu, S., He, M., Miao, J., and Peng, Y. (2023). Fault diagnosis method for imbalanced data based on multi-signal fusion and improved deep convolution generative adversarial network. *Sensors*, 23(5), 2542-2562.

Du, D., Wei, X., and Yang, L. (2023). Analysis of centralized control system for safety production and operation of distribution network. *Advances in Engineering Technology Research*, 6(1), 149-149.

Gao, W., Yu, L., Tan, Y., and Yang, P. (2022). MSIMCNN: multi-scale inception module convolutional neural network for multi-focus image fusion. *Applied Intelligence,* 52(12), 14085-14100.

Guo, Z., Hao, Y., Shi, H., Wu, Z., Wu, Y., and Sun, X. (2023). A fault diagnosis algorithm for the dedicated equipment based on the CNN-LSTM mechanism. *Energies*, 16(13), 5230-5251.

Han, S., Niu, P., Luo, S., Li, Y., Zhen, D., Feng, G., and Sun, S. (2023). A novel deep convolutional neural network combining global feature extraction and detailed feature extraction for bearing compound fault diagnosis. *Sensors*, 23(19), 8060-8066.

Han, Y. (2023). Wavelet analysis and consensus algorithm-based fault-tolerant control for smart grids. *Frontiers in Energy Research*, 11(1), 1160256-1160261.

Jalayer, M. (2022). Fault detection and diagnosis with imbalanced and noisy data: A hybrid framework for rotating machinery. *Machines*, 10(4), 237-255.

Jin, Y. (2022). Multisource Heterogenous Data Fusion for Fault Identification of Buried Substations. *Frontiers in Energy Research,* 10(1), 909520-909525.

Jin, Y., Chen, C., and Zhao, S. (2021). Multisource data fusion diagnosis method of rolling bearings based on improved

multiscale CNN. *Journal of Sensors*, 2021(1), 2251530.
Kafunah, J., Ali, I., and Breslin, G. (2021). Handling imbalanced datasets for robust deep neural network-based fault detection in manufacturing systems. *Applied Sciences,* 11(21), 9783-9786.
Lee, G., Kim, S., and Lee, H. (2024). Sound-Based Unsupervised Fault Diagnosis of Industrial Equipment Considering Environmental Noise. *Sensors*, 24(22), 7319-7324.
Lei, L. (2025). Research Progress on Data-Driven Industrial Fault Diagnosis Methods. *Sensors (Basel, Switzerland),* 25(9), 2952-2958.
Li, Z. (2022). Intelligent fault diagnosis method for industrial processing equipment by icecnn-1d. *Electronics*, 11(24), 4207-4212.
Liu, C. (2022). Technology development and commercial applications of industrial fault diagnosis system: a review. *The International Journal of Advanced Manufacturing Technology*, 118(11), 3497-3529.
Liu, M. (2023). Research on the Centralized Control System of Digital Platform Operators. *Frontiers in Humanities and Social Sciences*, 3(1), 42-51.
Meng, Q., Hussain, S., Luo, F., Wang, Z., and Jin, X. (2024). An online reinforcement learning-based energy management strategy for microgrids with centralized control. *IEEE Transactions on Industry Applications,* 61(1), 1501-1510.
Qin, H., Li, G., Lv, X., Guo, L., and Li, X. (2023). A Louver Exhaust Fan Centralized Control System with Predictive Maintenance. *Integrated Ferroelectrics*, 235(1), 56-67.
Wan, S. (2023). Bearing fault diagnosis based on multisensor information coupling and attentional feature fusion. *IEEE Transactions on Instrumentation and Measurement,* 72(1), 1-12.
Wang, J. (2021). Fault diagnosis of bearings based on multi-sensor information fusion and 2D convolutional neural network. *IEEE Access*, 9(1), 23717-23725.
Wang, Y., and Cao, G. (2023). A multiscale convolution neural network for bearing fault diagnosis based on frequency division denoising under complex noise conditions. *Complex & Intelligent Systems,* 9(4), 4263-4285.
Wenyun, N., Deshui, U., Xiaoni, G., Yong, G., Pengchang, G., and Haitao, O. (2022). Research on the centralized control system of aquaculture platform. *Fishery Modernization,* 49(5), 89-95.
Yan, W., Wang, J., Lu, S., Zhou, M., and Peng, X. (2023). A review of real-time fault diagnosis methods for industrial smart manufacturing. *Processes*, 11(2), 369-392.
Yang, X., Zhu, Y., Guo, Y., and Zhou, D. (2022). An image super-resolution network based on multi-scale convolution fusion. *The Visual Computer,* 38(12), 4307-4317.
Yongqiang, L., Yubao, F., and Chunhua, X. (2023). Research on Implementation and Application of CTC Regional Centralized Control System. *Railway Signalling & Communication Engineering*, 20(8), 1-7.
Yu, Q., Tolson, A., Shen, H., Han, M., Mai, J., and Lin, J. (2024). Enhancing long short-term memory (LSTM)-based streamflow prediction with a spatially distributed approach. *Hydrology and Earth System Sciences,* 28(9), 2107-2122.
Zhang, S. (2023). Robust failure diagnosis of microservice system through multimodal data. *IEEE Transactions on Services Computing,* 16(6), 3851-3864.
Zhang, X., Pan, X., Zeng, H., and Zhou, H. (2024). Intelligent diagnosis method for typical co-frequency vibration faults of rotating machinery based on sae and ensembled resnet-svm. *Chinese Journal of Mechanical Engineering,* 37(1), 64-68.
Zhang, Y., Muniyandi, R., and Qamar, F. (2025). A Review of Deep Learning Applications in Intrusion Detection Systems: Overcoming Challenges in Spatiotemporal Feature Extraction and Data Imbalance. *Applied Sciences*, 15(3), 1552-1557.
Zhao, M., Peng, H., Li, L., and Ren, Y. (2024). Multivariate Time Series Anomaly Detection Based on Spatial-Temporal Network and Transformer in Industrial Internet of Things. *Computers, Materials & Continua*, 80(2), 2815-2819.
Zou, Z., Chen, X., and Gong, H. (2025). Invisible and robust watermarking model based on hierarchical residual fusion multi-scale convolution. *Neurocomputing*, 614(1), 128834-128838.

Yi Xia was born in Chaohu, Anhui. P.R. China, in 1989. He received his master's degree from Hefei University of Technology, P.R. China. He currently works at State Grid Anhui Ultra High Voltage Company. His research interests include electric power system automation, centralized monitoring and control systems for substations, and cybersecurity of power systems.

Yao Xu was born in Shucheng, Anhui. P.R. China, in 1984. He earned his bachelor's degree from North China Electric Power University, P.R. China. He currently works at State Grid Anhui Ultra High Voltage Company. His research interests include electrical engineering and its automation.

Longgang Guo was born in Xianyang, Shaanxi. P.R. China, in 1985. He obtained his bachelor's degree from Zhengzhou University, P.R. China and MBA from Hefei University of Technology, P.R. China. He currently works at State Grid Anhui Ultra High Voltage Company. His research interests include substation operation and maintenance technology and power monitoring systems.

Cheng Xie was born in Tongcheng, Anhui. P.R. China, in 1993. She earned her master's degree from the University of Science and Technology of China. She currently works at State Grid Anhui Electric Power Co., Ltd. Her research interests include electric power systems and their automation, as well as automatic control engineering.

Huan Ma was born in Hefei, Anhui. P.R. China, in 1994. He received his master's degree from Southwest Jiaotong University, P.R. China. Now, he works at State Grid Anhui Ultra High Voltage Company. His research interests include electrical engineering and UHV (Ultra-High Voltage) technology.

Ling Weng was born in Chahu, Anhui. P.R. China, in 1985. He received his master's degree from Hefei University of Technology, P.R. China. He currently works at State Grid Anhui Ultra High Voltage Company. His research interests focus on relay protection in electric power systems.